ELSEVIER

Catalysis Today 76 (2002) 11–32

CATALYSIS TODAY

www.elsevier.com/locate/cattod

Synthesis and catalytic uses of carbon and silicon carbide nanostructures

Jean-Mario Nhut [a], Ricardo Vieira [a], Laurie Pesant [a], Jean-Philippe Tessonnier [a], Nicolas Keller [a,*], Gaby Ehret [b], Cuong Pham-Huu [a], Marc J. Ledoux [a]

[a] *Laboratoire des Matériaux, Surfaces et Procédés pour la Catalyse, UMR 7515 du CNRS, ECPM, Université Louis Pasteur, 25 rue Becquerel BP 08, 67087 Strasbourg Cedex 2, France*

[b] *Groupe Surface Interface, Institut de Physique et Chimie des Matériaux de Strasbourg, UMR 7504 du CNRS, Université Louis Pasteur, 23 rue du Loess, 67037 Strasbourg Cedex, France*

Abstract

Carbon nanofibers and nanotubes with controlled diameters were synthesized by catalytic decomposition of an ethane/hydrogen mixture over nickel and iron supported catalysts. The synthesis of the first silicon carbide (SiC) nanotubes was performed according to the shape memory synthesis (SMS) method. The benefit of using carbon and SiC nanotubes as catalyst supports was evidenced, respectively in the case of the selective C=C bond hydrogenation in the α,β-unsaturated cinnamaldehyde and the low temperature selective oxidation of H_2S into elemental sulfur (60 °C). Carbon nanotubes as support allowed to increase both cinnamaldehyde conversion and selectivity toward C=C bond hydrogenation. Supporting a nickel-based catalyst on SiC nanotubes allowed to increase both desulfurization activity of the catalyst and its solid sulfur storage capacity. The inner partial pressure concept, or confinement effect, was developed to explain the high performances of this new SiC-based catalyst. The last section is devoted to further objectives for developing such highly performing new support materials.

Keywords: H_2S oxidation; Cinnamaldehyde hydrogenation; Silicon carbide; Carbon; Nanotube; Nanofiber; Confinement effect

1. Introduction

Development of new supports for catalytic active phases is one of the most important research fields in heterogeneous catalysis. Industrial supports are usually based on high surface area γ-Al_2O_3, pure or doped, and carbon, support materials developed several decades ago. The main drawbacks of the alumina support are its mechanical and thermal instability, and the chemical interaction between the support and the active phase, leading to the decrease in catalyst performance by chemical reactions and hindering the recovery of the active phase at the end of the catalyst's lifetime [1–4]. In addition, alumina support is an insulating material which cannot disperse the heat released from its surface during the reaction or during oxidative regeneration performed in order to burn off the carbonaceous residues. It can lead to the formation of hot spots and thus to drastic modifications of the support and the nature of the active phase.

* Corresponding author. Tel.: +33-3-90-24-26-75; fax: +33-3-90-24-26-74.
E-mail address: nkeller@chimie.u-strasbg.fr (N. Keller).

0920-5861/02/$ – see front matter © 2002 Elsevier Science B.V. All rights reserved.
PII: S0920-5861(02)00206-7

The alumina support drawbacks can be overcome by using carbon-based materials which display higher thermal and chemical stability. Up to now, activated carbon has been widely used industrially as active phase support, especially in liquid phase processes, due to its possible separation from the reaction solution and its resistance towards aggressive media. Moreover, the metal of the supported phase could be relatively easily recovered after use. However, carbon support also suffers several drawbacks: low mechanical stability which induces the formation of fines during operation and high tortuosity with the presence of a large amount of micropores which could hinder the full accessibility of the reactants to the active site. Carbon-based materials also severely suffer from their low oxidation resistance which does not allow their use at high temperature under an oxidative atmosphere.

In order to overcome attrition problems under vigorously agitated liquids, which can lead to the loss of the active phase and to a decrease in the catalyst particle size, rendering less efficient the catalyst–liquid phase separation, an increasing interest was devoted to the development of new monodimensional supports such as carbon nanotubes (CNTs) or nanofibers. These nanostructured carbon-based materials display an exceptionally high mechanical strength, high thermal conductivity, medium to high specific surface areas and a high external surface area, which render them interesting candidates for use as catalyst supports instead of the traditional alumina and/or carbon-based materials.

Since the discovery of fullerenes in 1985 [5], a large part of the innovative carbon-based research was notably focused on the chemistry of sp^2-hybridised nanostructured carbon, both from a fundamental point of view and for potential applications [6–10]. The use of such carbon nanostructures as catalyst support seems to be one of the most promising applications. Recently, an increasing number of reports has been published on the use of such nanostructures as catalyst support for several reactions either in gas or in liquid phase media [11–15]. They displayed very interesting and unusual behaviors as compared to classical supports.

In parallel to its development for use in a broad range of applications including biomedical materials, high temperature semiconducting devices, optical elements and lightweight/high strength structures, silicon carbide (SiC) received growing interest as a support material in the catalysis field [16]. The high thermal conductivity, high resistance towards oxidation, high mechanical strength and chemical inertness, properties required for use as heterogeneous catalyst support and exhibited by SiC, allowed it to be a promising candidate to replace conventional industrial supports for several catalytic reactions. The main drawback of SiC, namely the very low surface area of the commercially available material, was overcome by the considerable attention focused on new preparative methods, allowing higher surface area carbides to be obtained [17–20]. Another drawback of SiC is the difficulty in its shaping as SiC prepared by the usual industrial method is in a powder form and is not directly suitable for use as catalyst support. Some years ago, Ledoux and coworkers [21–24] developed a new synthesis method for medium and high surface area carbides, called the shape memory synthesis (SMS). The synthesized materials could reach specific surface areas ranging between 20 and 200 m^2/g. The SMS method also allowed the preparation of SiC with controllable size and shape, by controlling the size and shape of the carbon-based precursor. Such control is a real advantage as compared to the traditional SiC, for which binders are required to obtain the final macroscopic shape. The SiC prepared according to the SMS method was very efficiently used for several reactions such as hydrodesulfurization [22], automotive exhaust-pipe reactions [25], isomerization of linear saturated hydrocarbons [26,27], *n*-butane dehydrogenation–isomerization [28,29] reactions and the selective oxidation of H_2S into elemental sulfur [30–33].

The aim of the present article is to report on the synthesis and catalytic use of carbon and SiC nanostructures. The first example concerns the low temperature selective oxidation of H_2S into elemental sulfur over nickel sulfide-based materials, used as test reaction to show the influence of the SiC support morphology on the catalytic behaviors. This very important reaction from an environmental point of view is studied in the laboratory [30–35]. This reaction takes place in the Claus Plant Tail-Gas Units. A second example will show the use of CNTs for liquid phase applications, in the case of the selective C=C bond hydrogenation of cinnamaldehyde. The precursor materials and cata-

lysts were characterized by different techniques, such as powder X-ray diffraction (XRD), surface area and porosimetry, scanning electron microscopy (SEM) and transmission electron microscopy (TEM) coupled with electron dispersive spectroscopy (EDS). Combination of the characterization and catalytic results will allow us to propose a new concept about the reaction pathways inside the support tubule.

2. Experimental

2.1. Carbon-based nanostructures

Purified CNTs supplied by Applied Science Ltd. (OH, USA) were used directly without any pretreatment. The primary structure of the CNTs consisted of pellets of about 10 μm in diameter. The CNTs had an outer diameter between 60 and 150 nm, an i.d. between 30 and 100 nm and lengths up to several hundred micrometers (Fig. 1a and b). Note the presence of an amorphous carbon layer on the outer surface of the CNTs which could be due to carbon formation by pyrolysis of the reactant mixture during the CNT synthesis (Fig. 1c). The CNTs had a specific surface area of 10 m^2/g with no microporosity. Residual metallic iron, with a concentration lower than 0.2 wt.% and used for CNT synthesis, is encapsulated inside the graphene layers, as indicated by the arrow in the TEM image (Fig. 1b). Those particles could thus not be accessible to the gas phase during any further treatments and reactions as reported in previous work [36].

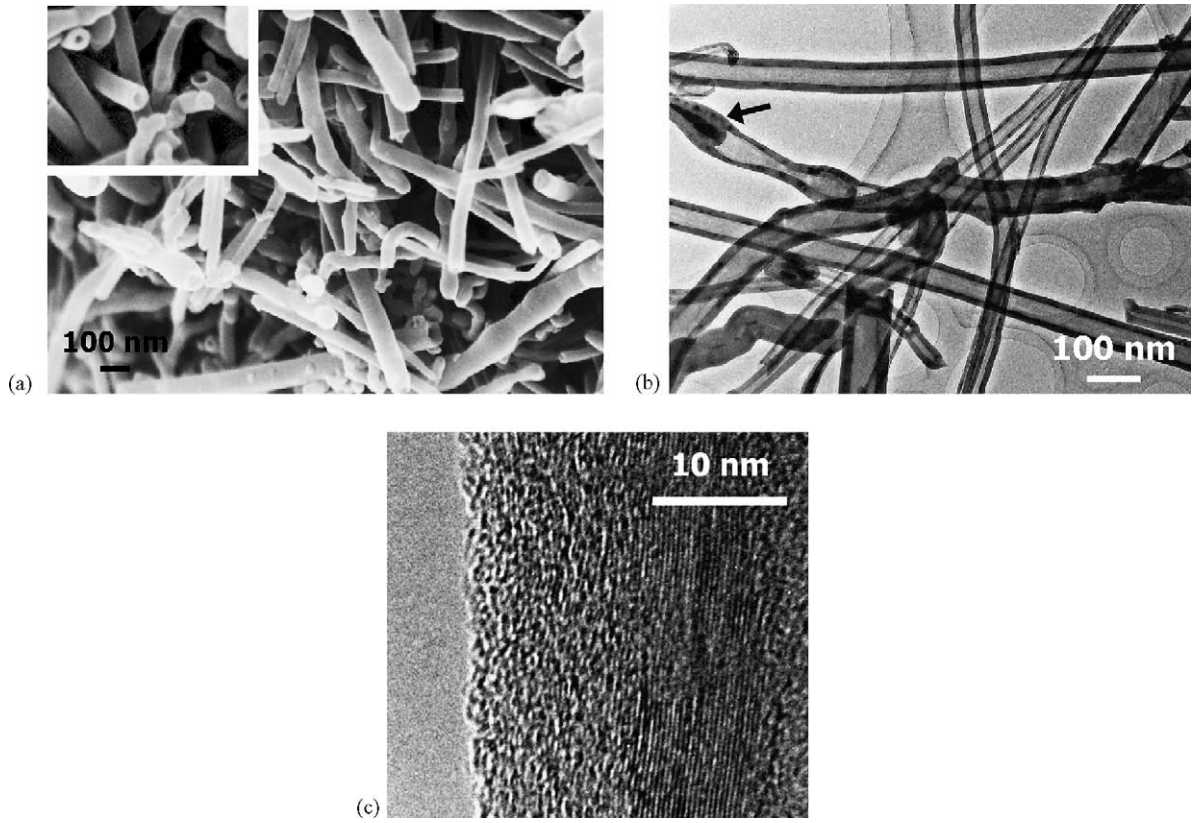

Fig. 1. The commercial CNTs purchased from Appl. Sci. Ltd.: (a) SEM image with inset focused on the open end of the tubes and (b) TEM image with a residual encapsulated iron particle indicated by the black arrow. Note the complete absence of nanoparticles inside the sample. (c) Higher resolution TEM image, showing the amorphous carbon layer on the outer surface of the CNTs.

Smaller CNTs were synthesized by the catalytic decomposition of an ethane and hydrogen mixture over a silica supported iron catalyst (20 wt.% of Fe) at 750 °C. Ethane was found to be the most appropriate gas, probably because it can provide the right balance of carbon as compared to hydrogen on the surface of the metal particle [36]. Jaeger and Behrsing [37] have reported that the nature of the gas phase could influence the growth rate, but did not influence the nature of the nanotubes. The subsequent CNT purification process consisted of flotation, followed by soda treatment at 80 °C for 12 h to dissolve the traces of the remaining support. A further aqua regia attack overnight under reflux to remove the last traces of iron, followed by several washings with distilled water up to neutral pH, provided ultrapure multiwalled nanotubes.

Carbon nanofibers were produced by the similar catalytic decomposition of ethane/H_2 over a supported nickel catalyst (20 wt.% on SiO_2 or γ-Al_2O_3) at 650 °C for several hours. Several groups have reported that Ni metal was the best catalyst to favor nanofiber synthesis [38,39]. The carbon nanofiber purification was achieved as described above for nanotubes.

2.2. SiC-based nanostructures

Description of the apparatus and crucible used in the SiC synthesis has been given in detail in previous extensive publications [24,40]. It involves the gas–solid reaction between SiO vapors and the solid carbon structure under dynamic vacuum around 1200–1300 °C, the generation of the SiO vapors being performed by heating a mixture of Si and SiO_2 at lower temperature. The SMS, developed some years ago by Ledoux and coworkers [41], allowed to obtain medium and high surface area SiC, starting from an appropriate carbon preform. The macrostructural features of the starting carbon determined the resulting SiC morphology (grains, extrudates, spheres, monoliths, etc.) leading to the SMS concept [16,22–24,40–42]. The macro- to microscale gap was recently bridged in previous works by applying the SMS to carbon microfibers with an outer diameter of 10 μm as starting carbon material [40,43]. SiC microtubes with a similar outer diameter and a controlled thickness of the walls were obtained.

The synthesis of SiC nanotubes was attempted by the SMS method, by using carbon nanostructures as preforms. Commercial and home-made CNTs and carbon nanofibers were submitted to the SiO vapor attack at 1200–1250 °C.

2.3. Catalyst preparation

The SiC nanotube supported nickel catalyst was prepared by incipient wetness impregnation of the SiC support with an aqueous solution of nickel nitrate ($Ni(NO_3)_2{\cdot}6H_2O$, Merck). The solid was dried overnight at room temperature and subsequently in an oven at 110 °C. The decomposition of the nitrate salt to form its corresponding oxide was achieved by further calcination in air at 350 °C. Sulfidation at 300 °C under H_2S (4 wt.%) in flowing He allowed to form the supported NiS_2 catalyst, as described in previous publications for similar materials [34,35]. The nickel loading measured by atomic absorption spectroscopy (AAS) was 5 wt.%.

The CNTs supported palladium catalyst was prepared by wet impregnation of the dried support (10 g) with an aqueous solution (40 ml) of palladium nitrate ($PdNO_3{\cdot}5H_2O$, Strem Chemicals). The slurry was dried in air at 100 °C overnight and then calcined at 400 °C in air for 2 h in order to decompose the palladium salt. The calcined catalyst was further reduced under flowing hydrogen at 400 °C for 2 h and then stored in a vial in air. The palladium loading measured by AAS was 5 wt.%.

2.4. Characterization techniques

The metal loading was analyzed by AAS performed at the Service Central d'Analyse of the CNRS, Vernaison, France.

Structural characterization of the samples was done by powder XRD measurements, carried out with a Siemens Diffractometer model D-5000, using Cu Kα radiation and operated at 40 kV and 20 mA. The measurements were made with long time scans (10 s) and a small step scan ($2\theta = 0.02°$). The nature of the crystalline phase in the sample was checked using the data base of the Joint Committee on Powder Diffraction Standards (JCPDS).

The surface area measurements were performed on a Coulter SA-3100 porosimeter using N_2 as adsorbent.

Before each measurement, the sample was transferred into the BET cell via a glove-box under dry nitrogen. The cell was equipped with a greaseless valve in order to avoid air exposure of the sample during the transfer to the porosimeter. S_{BET} is the surface area of the sample calculated from the nitrogen isotherm using the BET method. The micropore surface area and volume were calculated using the *t*-plot method developed by de Boer [44]. The *t*-plot consists of the analysis of the v_l–*t* plot curve where v_l is the volume of nitrogen adsorbed as liquid at a given pressure P/P_0 by the BET surface and *t* is the statistical thickness obtained by dividing the volume of nitrogen adsorbed as liquid at a given pressure P/P_0 by the BET surface. A more detailed study has been published by Mikhail et al. [45] concerning the correctness of the different parameters used in this method.

The morphology of the materials was observed by SEM using a Jeol microscope Model JMS-840 operated at 20 mA with an accelerating voltage of 20 kV. Before observation, the samples were coated with a thin layer of carbon in order to avoid a charge effect phenomenon.

TEM and EDS were carried out in a Topcon Model EB200B operating at 200 kV with a point to point resolution of 0.17 nm. Great care was taken during the TEM experiments in order to avoid heating effects from the incident beam. EDS analysis was carried out with a 5 nm and 100 s life time electron beam. The detector was equipped with beryllium windows.

2.5. Catalytic micropilots

2.5.1. Low temperature selective H_2S oxidation

Selective oxidation of H_2S was carried out in the apparatus working at atmospheric pressure already described in detail in previous work [30,33]. The catalysts were tested at a temperature of 60 °C in a fixed-bed mode, with a reactant feed containing 2000 ppm vol. of H_2S, 3200 ppm vol. of O_2, 20 vol.% H_2O and balance He, corresponding to a O_2 to H_2S molar ratio of 1.6 and a weight hourly space velocity (WHSV) ranging between 0.007 and 0.043 h^{-1}. The steam was provided by a saturator kept at the required temperature. At such a low temperature, a large fraction of the steam condensed at the head of the reactor, and the reaction was performed in a trickle-bed mode. In order to avoid condensation (except in the reaction zone), all the lines were maintained at 120 °C with heating tapes. The analysis of the inlet and outlet gas were performed on-line using a Varian CX-3400 gas chromatograph (GC) equipped with a Chrompack JSQ capillary column allowing the separation of O_2, H_2S, H_2O and SO_2, a catharometer detector and a calibrated six port loop (500 μl). SO_2 was also measured by means of a specific detector (Dräger model 81-01531) allowing the detection of SO_2 in a range of concentrations between 10 and 5000 ppm and previously calibrated using a known amount of SO_2.

2.5.2. Hydrogenation test

The hydrogenation of cinnamaldehyde (CALD) was carried out at atmospheric pressure and low temperature (80 °C) in a microreactor. The solution contained 40 ml of dioxane, 10.5 g of reactant and the catalyst, corresponding to 6.25×10^{-3} g of Pd. Dioxane was used instead of alcohol in order to avoid any homogeneous reactions which could lead to the formation of heavier by-products [46–50]. Argon at room temperature bubbled through the liquid phase which was stirred for 1 h in order to remove traces of dissolved oxygen in the medium, before introducing the catalyst and switching to the hydrogen flow. This hydrogen flow was continuously fed through the liquid phase (10 cm^3/min), kept under vigorous stirring (500 rpm) for 1 h at room temperature before increasing the reaction temperature. The hydrogen stream was regulated by a Brooks 5850 TR mass flowmeter linked to a Brooks 5876 control unit. The cinnamaldehyde concentration and the product distribution were followed as a function of time on stream by gas chromatography analysis of microsamples periodically drawn and diluted by dioxane. It was performed on a Varian 3400-CX GC equipped with a PONA capillary column coated with methyl siloxane (Hewlett-Packard, length 50 m, 0.2 mm i.d., film thickness 0.5 mm) and a flame ionization detector (FID). The products were calibrated by using pure components, i.e. cinnamaldehyde, cinnamyl alcohol, 3-phenylpropyl alcohol and 3-phenylpropionaldehyde (ACROS, purity >98%) diluted in dioxane. The analytical error calculated from the GC was within 2%. The conversion and product distribution were calculated from the GC analysis. Cinnamaldehyde (ACROS) was used as-received. GC analysis indicated a purity of 98.8%, the major organic impurities being cinnamyl alcohol (0.1%),

3-phenylpropyl alcohol (0.2%). H_2 (Air Liquide, grade U) was used as-received.

3. Results and discussion

3.1. Synthesis of carbon nanostructures

TEM micrographs of the CNTs synthesized over the iron-based catalyst after the required purification process are presented in Fig. 2. They displayed an average i.d. ranging from 5 to 10 nm and outer walls corresponding to 8–10 graphene layers separated by a distance of 0.34 nm. The graphene layers which constitute the wall of the nanotubes were not so straight and parallel as compared to nanotubes obtained by other methods such as high temperature arc-discharge. This greater disorder between carbon planes was assigned to the relatively low temperature catalytic growth process. It should also be noted that almost no amorphous carbon was found on the outer surface of the home-made CNTs, as compared to commercial CNTs, highlighting the lack of pyrolytic carbon formation during the synthesis conditions used in the present work.

Fig. 3 shows carbon nanofibers obtained over the nickel-based catalyst. The low magnification image reveals that the nanofibers had an average outer diameter of 40–50 nm with lengths up to several tens of micrometers. The high resolution transmission electron microscopy (HRTEM) image shows the highly disorganized structure of the nanofibers along the axis, the herringbone structure corresponding to graphene planes sometimes connected in the middle of the fiber and forming a close angle of ca. 75°. The interplanar distance between two graphene layers was still at 0.34 nm, similar to that observed on the CNTs. The carbon nanofibers had a specific surface area between 100 and 250 m^2/g depending on the synthesis parameters [36]. The relatively high surface area of the carbon nanofibers compared to that of the CNTs, i.e. 250 m^2/g instead of 10 m^2/g, was directly attributed to the presence of highly reactive prismatic planes of the carbon nanofibers. They display a high density for gas adsorption as compared to the exposed basal planes of graphite in the CNTs. However, it should be noted that the surface area obtained here was still low compared to those reported generally in the literature, i.e. >500 m^2/g. Such a discrepancy in terms of surface area could be explained by the more ordered arrangement

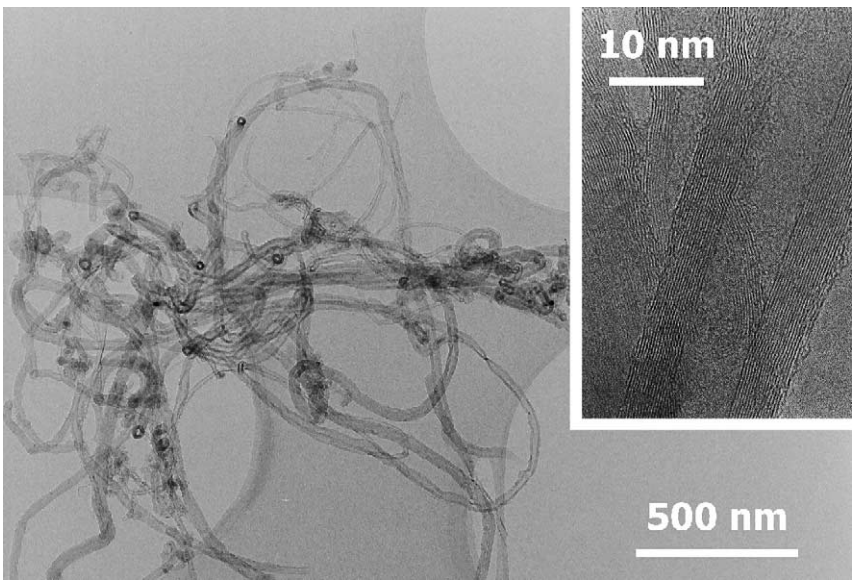

Fig. 2. TEM image of home-made small uniform CNTs (5–10 nm i.d.) obtained by catalytic decomposition of ethane and hydrogen over a silica supported iron catalyst. Inset: high resolution image shows evidence of the parallel orientation of the graphene planes with respect to the axis of the tubes.

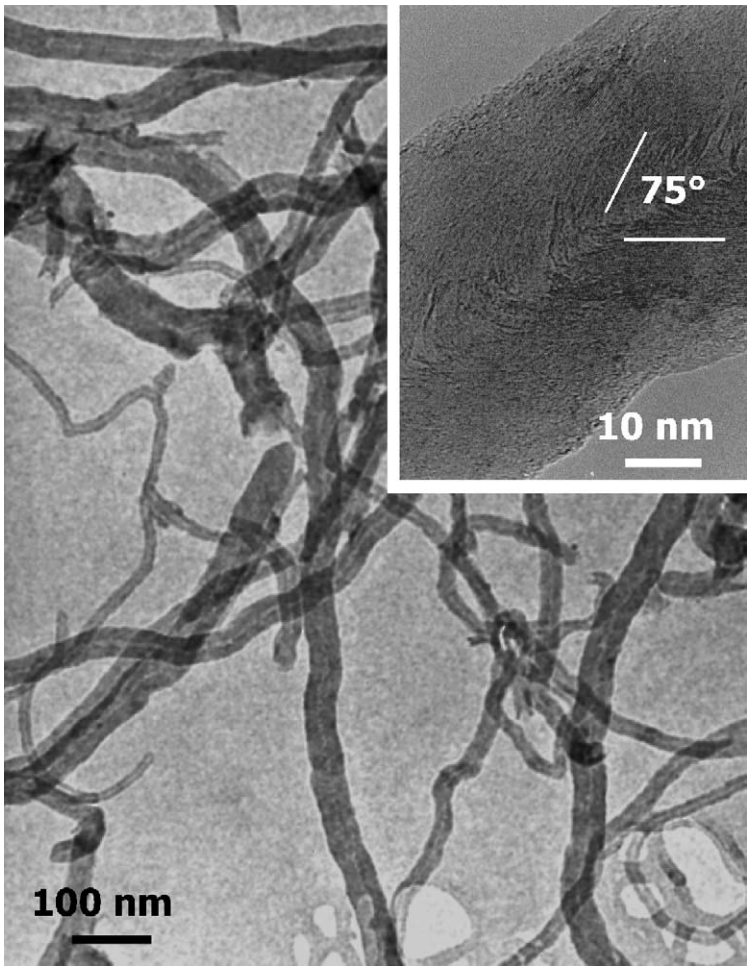

Fig. 3. SEM image of carbon nanofibers obtained by catalytic decomposition over a nickel supported catalyst. Inset: high resolution TEM image showing the herringbone structure oriented with an angle of 75° between them. The exposed planes are exclusively constituted by prismatic edges.

between the different graphene sheets in the present material.

It is worth noting the very high selectivity of the synthesis for nanofibers and nanotubes: almost no traces of other carbon species were detected, as compared to other synthesis methods such as carbon-arc production or plasma decomposition, where amorphous carbon and nanoparticles were also obtained in a significant amount [51–54]. The high selectivity towards carbon nanostructure formation is one of the most important conditions, required for their subsequent large scale production in order to avoid any further delicate, time and cost-consuming purification processes.

3.2. Synthesis of SiC nanotubes

The SiC nanotubes obtained using the commercial CNTs as starting material were first calcined at 600 °C in air to burn the remaining unreacted core carbon, according to the principles described in previous publications [24,40]. The SEM pictures presented in Fig. 4 evidence the concept of SMS. However, it should be noted that the smooth surface of the CNTs

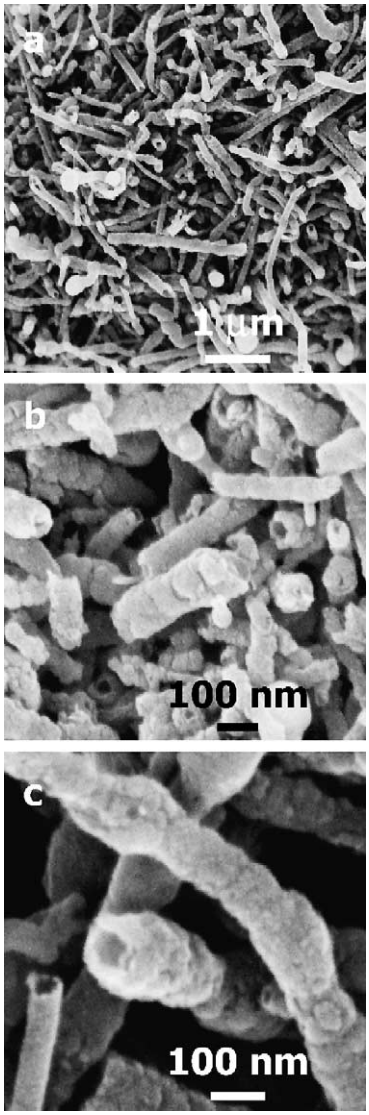

Fig. 4. SEM images of SiC nanotubes obtained by SMS using commercial CNTs as starting material. The smooth surface of the starting carbon was transformed into a more irregular one with holes and cracks.

was transformed after carburisation into a rougher one where holes and cracks could be seen at high magnifications (Fig. 4b and c). The loss of one carbon atom as CO gas along with the density change when going from C to SiC was probably responsible for the formation of such a disordered structure. No closure of the tube tip occurred during the synthesis, both inner and outer surfaces of the tubes remaining accessible for further treatments (Fig. 4c). The SiC nanotubes had an i.d. ranging between 30 and 100 nm. The purity of the synthesized material was confirmed by the XRD pattern, which only exhibited the diffraction lines corresponding to the β-SiC phase, crystallized in a face centered cubic structure (Fig. 5). No traces of other compounds such as silicon or silica were detected, meaning that such compounds, if present, were only in an amorphous form or in very small amounts.

The use of smaller home-made CNTs (5–10 nm i.d.) as carbon source for the SMS method did not allow the synthesis of smaller SiC nanotubes. Apparently, the relatively thin wall (8–10 carbon layers) was not strong enough to resist the simultaneous internal and external attacks on the CNTs by the hot SiO vapors. The SiO treatment led to the destruction of the tube morphology and only SiC powder was obtained.

Carbon nanofibers synthesized over the nickel-based catalyst were used instead of nanotubes as starting carbon-based material for the synthesis of the SiC nanotubes in the same reaction conditions. The low resolution TEM image showed that nanotubes synthesized at 1200 °C were still accompanied by a non-negligible amount of SiC powder (Fig. 6). This probably resulted from the destruction during the reaction of some carbon nanofibers which were not strong enough. XRD displayed the diffraction pattern of the β-SiC structure (not shown), but remained an ambiguous characterization, because of the presence of SiC powder among the nanotubes. The SiC nature of the nanotubes was proven by performing EDS on both small and large isolated nanotubes, which indicated the presence of both silicon and carbon inside the material (Fig. 6). A higher resolution TEM picture displayed the structure of the SiC nanotubes, i.e. similar one-dimensional morphology as the starting hollow carbon nanofibers (Fig. 7). The TEM micrograph revealed that with the retention of the gross morphology, the outer surface of the material was highly disordered (indicated by arrows) as compared to that of the starting carbon nanofibers. Such a phenomenon could be explained by (i) the rapid adsorption-reaction between the SiO vapour and the exposed prismatic planes of the carbon nanofibers, resulting in the

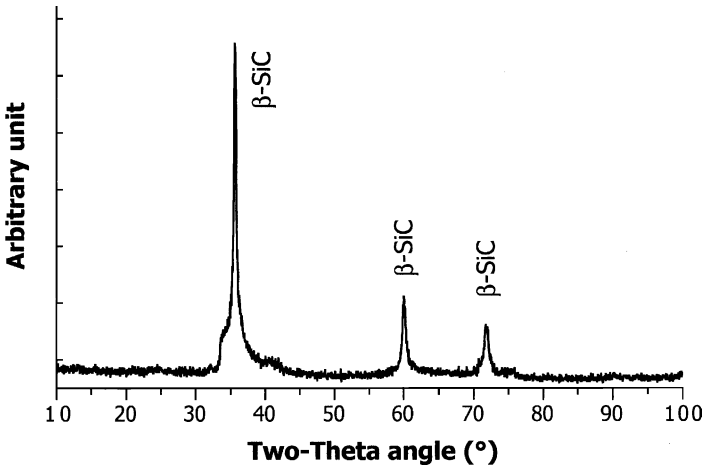

Fig. 5. XRD pattern of β-SiC nanotubes obtained by SMS using commercial CNTs as starting material.

formation of several nuclei along the fiber axis, and (ii) diffusion through the material of both the SiO vapour and the CO produced. It would lead to some local structure collapse with a concomitant formation of holes and cracks as has already been observed by SEM in the case of SiC nanotubes prepared from the commercial CNTs presented above and for SiC microtubes previously published [41]. HRTEM micrograph (low right corner inset) clearly evidenced the presence of some ordered domains inside the material with a different structure: the new almost parallel arrangement of the stacking planes inside the carbide material as compared to the 75° oriented planes in the former carbon nanofibers. However, some small darker areas were visible, attributed to a different thickness of the material for the electron beam, and would be a direct view of holes and porosity created in the SiC walls. The thin thickness of SiC nanotubes as compared to other SiC forms (grains, microtubes or bigger nanotubes) probably enhanced such phenomena, due to the structural fragility of the material. It would thus allow such nanoporosity to be observed by HRTEM, contrary to other macroshaped SiC material previously studied. Such visualization of the porosity was advanced by Bouchy in the complete HRTEM characterization of a molybdenum oxycarbide catalyst [55].

It is worth noting that the SMS method allowed the transformation of the carbon nanofibers into open nanotubes without modifying the gross morphology of the material (Fig. 8). Parallel to the SiO vapor attack on the nanofibers, migration of the internal carbon towards the surface occurred, due to the presence of an oxidizing agent (SiO) and this in turn, led to the formation of a hollow core. Such a phenomenon was already observed in the synthesis of molybdenum and vanadium carbide microtubes and explains why it was not necessary to open the tubes before performing the SiC synthesis. The nanotubes obtained had external diameters ranging from 10 to 100 nm, with an average diameter of 30 nm. The average internal diameter was of about 15 nm. The high degree of disorganization observed along the carbon nanofiber axis (increasing the accessibility to carbon atoms for the SiO molecules) and the small thickness of the nanofibers as compared to the commercial CNTs explained the total C → SiC transformation, and no further oxidation was required to obtain pure SiC. The SiC nanotubes had a specific surface area of about 40 m^2/g without any microporosity. The decrease in the specific surface area of the material when going from carbon nanofibers to SiC nanotubes could be explained by the local structure collapse during the synthesis and also by the surface diffusion which probably occurred due to the high synthesis temperature required. The complete transformation of the exposed prismatic planes of the carbon nanofibers, which were probably more available for adsorption of nitrogen gas, into the SiC structure could also be responsible for such a surface area decrease.

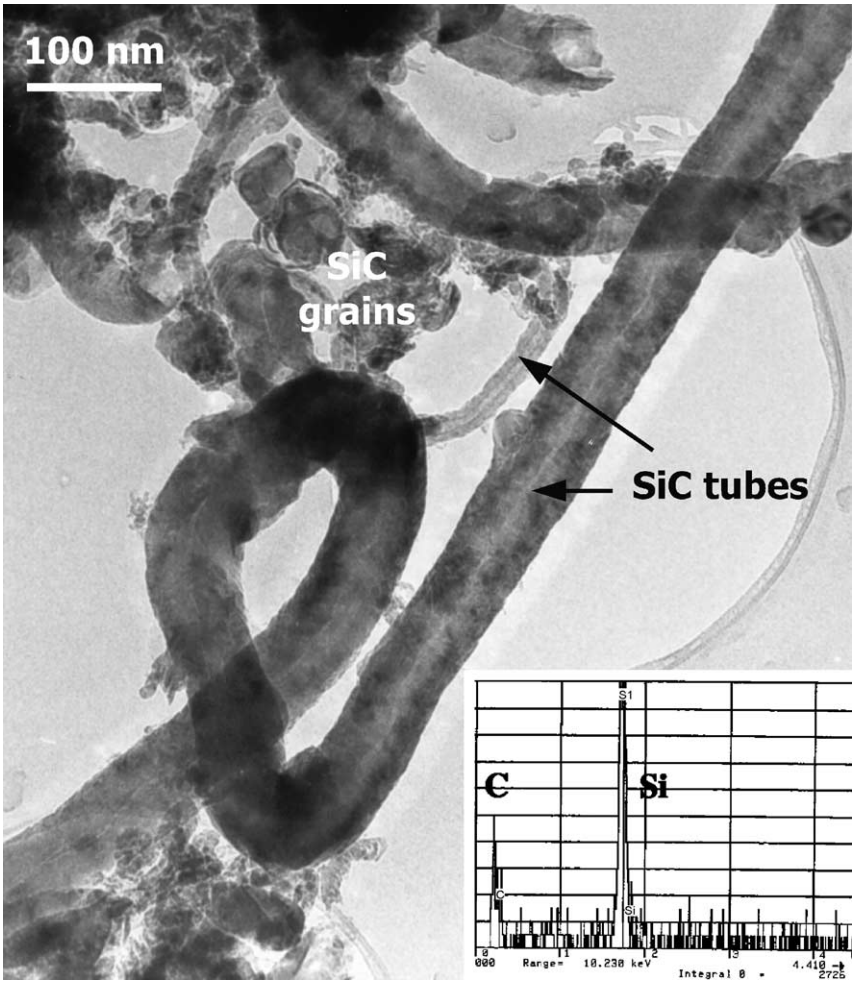

Fig. 6. TEM image of SiC nanotubes obtained by SMS using carbon nanofibers as starting material. Inset: EDS analysis on both small and large SiC nanotubes.

3.3. The use of SiC and CNT-based catalysts

3.3.1. The use of SiC nanotubes

The interest in the catalytic performance of SiC nanotubes compared to that of traditional SiC grains was shown in the case of the selective oxidation of H_2S into elemental sulfur at low temperature (60 °C). It has been reported in previous works that the use of a new type of support, i.e. SiC, and a nickel-based active phase allowed an active, extremely selective and stable catalyst to be obtained [30,32,34,35]. The superficial transformation of the starting NiS_2 supported phase into a very active nickel oxysulfide phase was proposed to explain the exceptional catalytic results obtained.

Most of the NiO phase, and also after the sulfidation step, its corresponding NiS_2 phase, was located inside the SiC nanotubes, as TEM images only showed a few NiO particles on the outer walls of the tubes. The thickness of the SiC nanotubes made the material not transparent enough for the electron beam, and did not allow the direct observation of nickel-based phases inside the tubes. EDS carried out on isolated SiC nanotubes however proved the presence of nickel inside the tubules (Fig. 9).

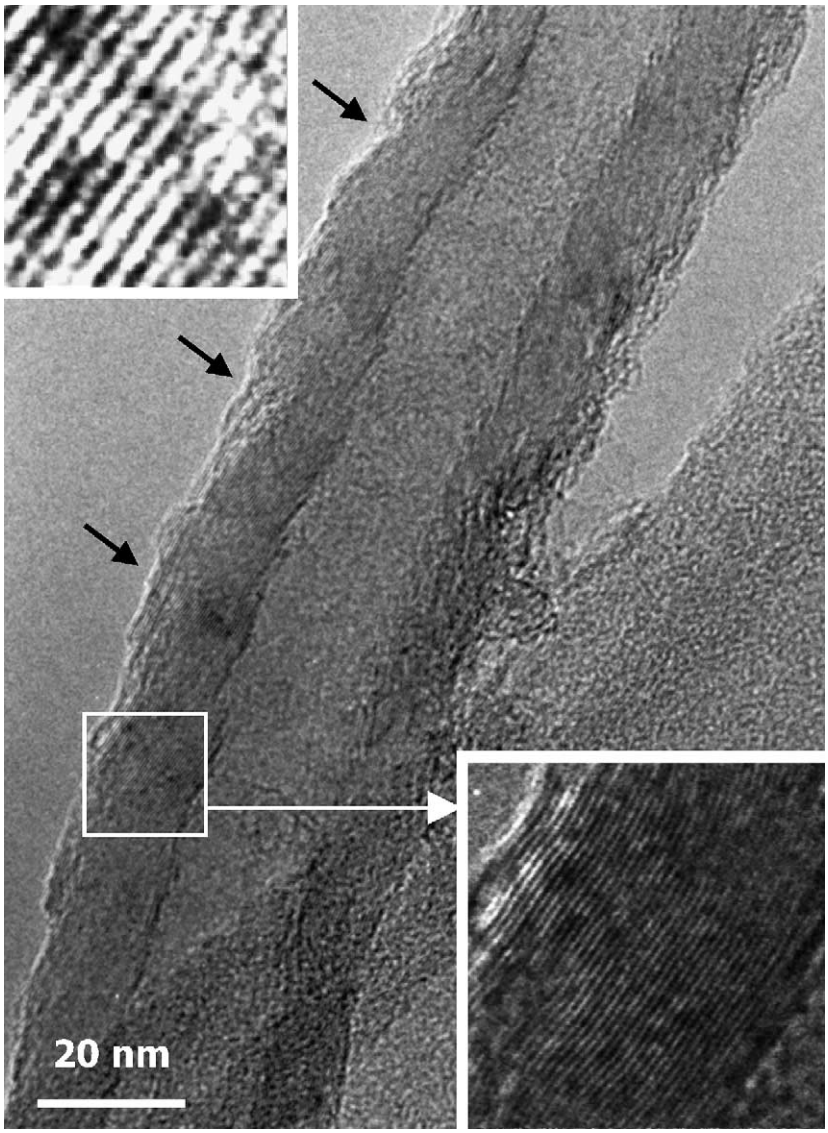

Fig. 7. TEM images of a SiC nanotube and highly contrasted HRTEM image of the SiC walls, evidencing the nanoporosity of the walls (insets).

The influence of the WHSV on the H_2S conversion obtained at 60 °C with the NiS_2 catalyst supported on SiC grains is shown in Fig. 10a. Whatever the total flow rate, the selectivity for elemental sulfur remained at 100%, no SO_2 being detected at the outlet of the reactor. Previous work showed that it could be explained by the low temperature used and the absence of any detrimental microporosity in the catalyst supported on β-SiC [30,31,34,35]. For a velocity of 0.007 h^{-1}, the catalyst showed a H_2S conversion of 100% from the beginning of the test and for more than 100 h of time on stream. Performing the test at higher velocity, i.e. 0.02 h^{-1}, led to completely different behavior in terms of activity. Indeed, after an activation period of a few hours, the H_2S conversion only reached a level of about 95%, and then deactivation rapidly occurred

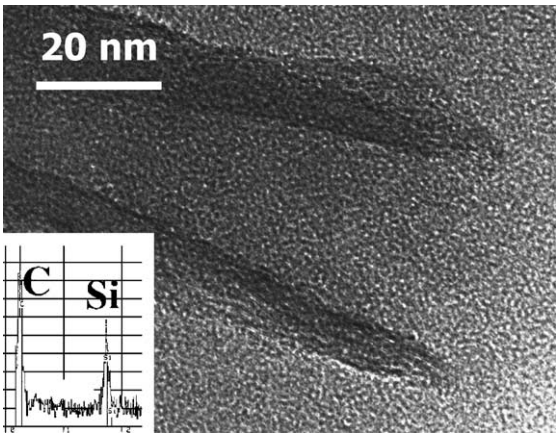

Fig. 8. TEM image and EDS analysis of the open end of a SiC nanotube.

with time on stream, and the catalyst was totally inactive after 50 h of reaction. Fig. 10b showed the benefit of the use of SiC nanotubes as support for the NiS_2 phase. At the high WHSV of 0.02 h^{-1}, the SiC nanotube supported catalyst still exhibited a H_2S conversion of 100% from the beginning of the test and no deactivation was observed, even for more than 100 h of time on stream, after which the weight of accumulated solid sulfur on the material was greater than 200 wt.% of the initial weight of the catalyst. A temporary increase in the WHSV from 0.02 to 0.043 h^{-1} led to a slight decrease in the H_2S conversion. The conversion also dropped to 94%, a value similar to that

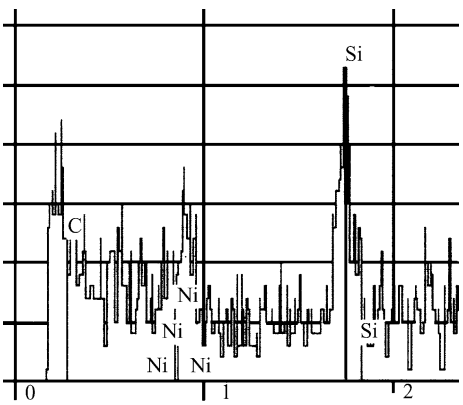

Fig. 9. EDS analysis of an individual SiC nanotube, evidencing the presence of nickel after the impregnation and calcination steps.

obtained with the SiC grains by using a lower WHSV of 0.007 h^{-1}.

It is worth noting that the use of SiC nanotubes allowed significant improvement in both the activity of the catalyst and the solid sulfur storage capacity for the low temperature oxidation of hydrogen sulfide. The improvement in the storage capacity of the catalyst was attributed to the increase in the free volume of the nanotube material, which remained available for sulfur storage during the reaction, as compared to the traditional grain size material. Indeed, previous work reported that the performances of catalysts supported on SiC grains for the selective H_2S oxidation are due to the mechanical removal of the sulfur formed from the active sites by a water film. The role of condensed water, acting as a conveyor belt on the catalyst surface has been already reported in detail in previous publications with similar catalysts supported on SiC grains [30,33–35]. The water allowed the sulfur formed to be removed from the NiS_2 active sites before the subsequent storage on hydrophobic SiC surfaces, outside the pores, which are free of active phase. Taking into account that the void volume outside the tubes is much larger than outside the pores of usual mesoporous SiC grains, larger amounts of sulfur could also be stored in the external void volume, after the evacuation of solid sulfur outside the nanotubes by water according to the same conveyor belt process, and where only very few NiS_2 particles are located. Fig. 11 shows SEM images of the SiC nanotube supported NiS_2 active catalyst after test and loaded with 200 wt.% of solid sulfur. The presence of solid sulfur outside the SiC tubes was clearly evidenced, although only very few particles of active phase were found on the outer walls of the catalyst. It confirmed that sulfur formed inside the SiC tubules was transported and then stored outside the tubular structure.

Baker and coworkers proposed that the peculiar activity obtained for graphite nanofiber supported nickel catalysts for the hydrogenation of butadiene or crotonaldehyde [11,13] was due to the specific morphology adopted by the nickel phase and induced by the nanofiber support. Using a very different kind of support, i.e. SiC nanotubes, there was no evidence in the present study for the flat hexagonal morphology observed by Baker and coworkers on graphite nanofibers. It appeared also interesting to develop a new idea, in order to explain the gain in activity when

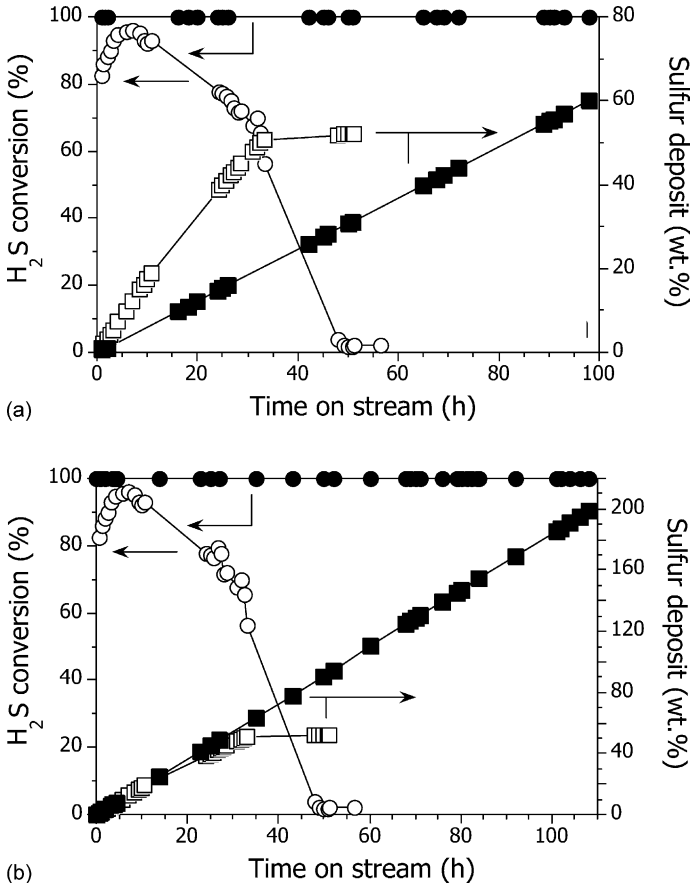

Fig. 10. H_2S conversion and the corresponding solid sulfur deposit on the surface as a function of time on stream at 60 °C: (a) obtained on the NiS_2 catalyst supported on SiC grains for WHSV = 0.007 h^{-1} (filled symbols) and WHSV = 0.02 h^{-1} (open symbols); (b) obtained for WHSV = 0.02 h^{-1} with the SiC nanotubes (filled symbols) and the SiC grains (open symbols) as support.

using the nanotube morphology as support: the inner partial pressure concept, or confinement effect, due to the peculiar tubular morphology of the material.

3.3.2. *The inner partial pressure concept*

The increase in WHSV led to a significant decrease in the H_2S conversion on the catalyst supported on SiC grains. It could not be due to the amount of solid sulfur accumulated on the catalyst surface, according to previous results which showed that the catalytic desulfurization activity was not affected by the amount of solid sulfur deposited on the catalyst surface up to about 100 wt.% [30]. The deactivation probably occurred in the present study because H_2S molecules could not be adsorbed on the active site to further react with O_2, due to the decrease in contact time, following an usual kinetic behavior. In an extended review, Pieplu et al. [56] recently summarized kinetic studies related to the direct and selective H_2S oxidation by O_2 to elemental sulfur. According to a traditional rate law with positive reaction order relative to H_2S, the increase in WHSV would be compensated by an increase in the H_2S partial pressure on the catalytic sites, in order to recover a high reaction rate, i.e. H_2S conversion. It led to the development of a new concept of the selective increase of the reactant partial pressure inside the nanotube, on or next to the active site due to the peculiar morphology of the support.

The inner partial pressure concept is based on the large increase in the H_2S partial pressure inside

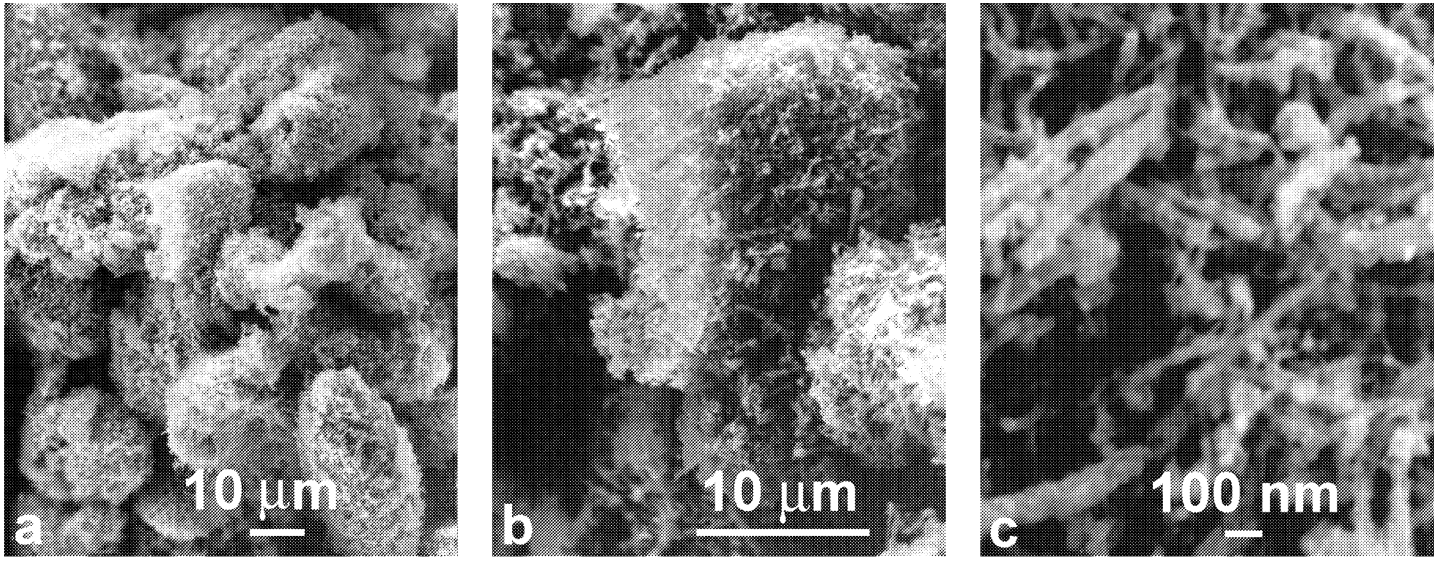

Fig. 11. SEM images of the SiC nanotube supported NiS_2 catalyst with a solid sulfur loading of 200 wt.% after more than 100 h of time on stream at 100% conversion.

the SiC nanotubes, probably by a microcapillarity phenomenon. In this concept, the apparent macroscopic H_2S partial pressure would remain unchanged, outside the nanotubes, whereas the microscopic or nanoscopic partial pressure would significantly increase inside the nanostructure. Such modification of the reactant partial pressure probably occurred during the flow through the tube, due to a tube wall effect and segregation phenomena between the different gaseous products. According to such a concept, one should expect that compounds with a high dipolar moment, i.e. H_2S which is the least concentrated of the reactants, would be the most affected during the diffusion through the tubule. A similar concept has been proposed by different authors for the use of CNTs to improve hydrogen storage capacities [57,58]. In the present study, the use of SiC instead of carbon and of H_2S as inlet reactant, a molecule presenting a permanent dipole, instead of more "inert" H_2 molecules in term of interactions with the surface, would both lead to more visible effects than in the papers cited above. With respect to the nature of the nanotubes used, it has been reported in previous work that the surface of SiC grains or microtubes was partially covered by a 1–3 nm thick layer of a mixture of silica and silicon oxycarbide, giving hydrophilic properties to some parts of the SiC surface layer [30,34,35,41]. The local formation of this oxygen-containing surface layer occurred on the high Miller index planes, presenting a higher density of defects, during the SiC synthesis by the SMS method. It is probable that such a hydrophilic layer was also formed during the synthesis of the SiC nanotubes. The carbon nanofiber to SiC nanotube transformation, along with the nanostructure opening, could even favor such a partial oxidation of the inner SiC layer, due to the probable high defect density of the inner SiC nanotube surface (Fig. 7). The highly hydrophilic nature of the nanotube inner surface would also increase the microcapillarity phenomenon.

3.3.3. *The catalytic use of CNTs*

The liquid phase selective hydrogenation of the C=C bond in the α,β-unsaturated cinnamaldehyde was studied to show the benefit of the use of the CNTs support versus the traditional powder activated charcoal-based catalyst. The CNTs supported palladium catalyst was compared to a commercially available high surface area activated charcoal supported palladium catalyst (5 wt.%) supplied by Aldrich (1000 m^2/g). The HRTEM micrographs presented in Fig. 12 evidenced the high and homogeneous dispersion of spherical palladium metal particles inside the tubule of the CNTs support. The average particle size distribution was centered around 3–5 nm in diameter. It was worth noting that 95% of the particles were located inside the carbon tubule. The almost exclusive location of the metal particles inside the tubes could be explained by the fact that during the impregnation process, the liquid completely filled the inner part of the support due to the probably higher hydrophilicity of the inner surface as compared to that of the outer surface. Results reported in the literature have shown that CNTs could easily be filled with low surface tension liquids, i.e. $<$190 mN/m [59]. Water, with a surface tension of 72 mN/m, would thus wet and rapidly fill the inner part of the tube. The further thermal treatments, calcination and reduction, led to the formation of metal particles decorating the inner part of the tube according to the results reported above. The ability of the low surface tension liquid to fill the inner part of the CNTs also strongly depended on the tubule diameter according to work reported by Ugarte et al. [60]: the smaller the inner tubule, the lower the filling efficiency. However, as will be shown in the last part of this paper, the CNTs filling efficiency was not only due to the surface tension of the liquid but also to other parameters which seem to be more difficult to evidence.

The activated charcoal-based catalyst exhibited a similar palladium metal particle dispersion, centered at around 3–5 nm. However, TEM observation showed that on such a catalyst the metal particles were frequently found as aggregates, which was not the case for the CNTs catalyst.

The reaction pathway involved in the hydrogenation of cinnamaldehyde is shown in Fig. 13. Catalyst performances obtained as a function of time on stream over the palladium catalysts, supported on the commercially available high surface area activated charcoal and the CNTs are shown in Fig. 14. The use of the CNTs as support allowed a slight increase in the disappearance rate of the cinnamaldehyde. The disappearance of the cinnamaldehyde was achieved after 33 h of time on stream over the CNTs, as compared to 40 h for the commercial catalyst.

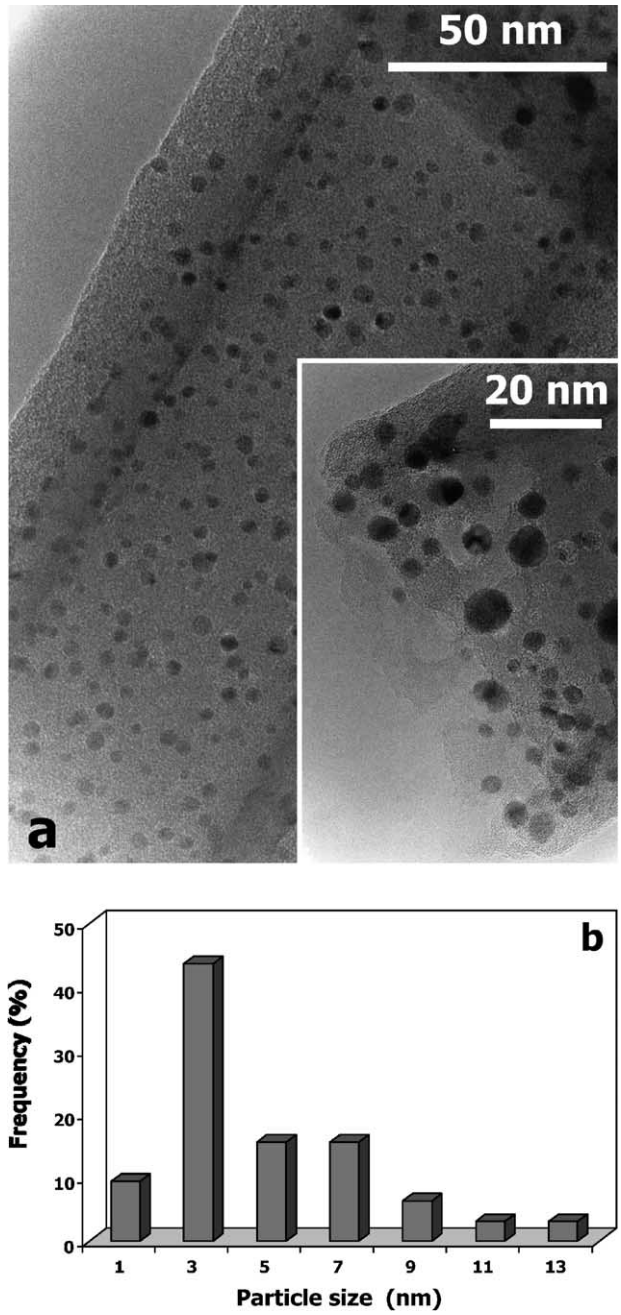

Fig. 12. HRTEM images of the CNT supported palladium catalyst (a) and the derived particle size distribution, obtained on a statistical sample of TEM micrographs (b).

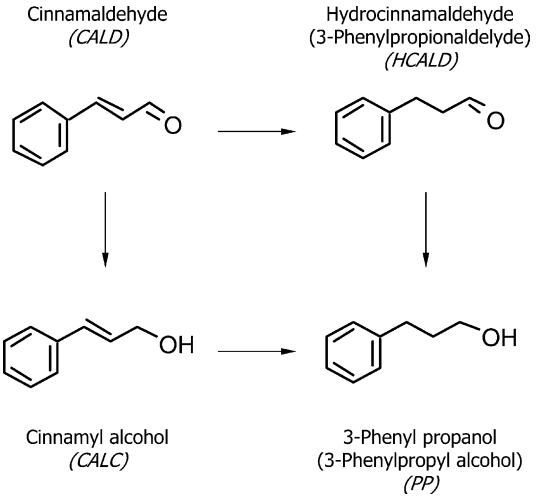

Fig. 13. Reaction pathway of the hydrogenation of cinnamaldehyde.

According to the TEM observations which did not show any significant differences in the metal particles, the slight increase in the disappearance rate of cinnamaldehyde on the CNTs-based catalyst could be explained by the high surface-to-volume ratio of the CNTs as compared to the activated charcoal grains. The mass transfer phenomenon, predominant in liquid phase reactions, was significantly decreased because of the small size of the CNTs, i.e. a few tens of nanometers compared to several micrometers for the activated charcoal. The absence of any microporosity could moreover increase the accessibility of the active sites for the reactants. The low specific surface area of the CNT supported catalyst (10 m^2/g) as compared to the corresponding very high surface area catalyst (1000 m^2/g) could explain why the gain in activity remained nevertheless quite small [13,38,61,62].

More significant was the large increase in the selectivity towards the C=C bond hydrogenation by using the CNT support. It led to the formation of 80 vol.% of the saturated aldehyde (hydrocinnamaldehyde) and 20 vol.% of the totally hydrogenated phenyl propanol. For comparison, both saturated alcohol (corresponding to the hydrogenation of C=O and C=C bonds) and aldehyde were obtained in similar amounts on the commercial highly microporous catalyst (55:45). In both cases, traces of the unsaturated alcohol were not detected whatever the conversion over the catalyst

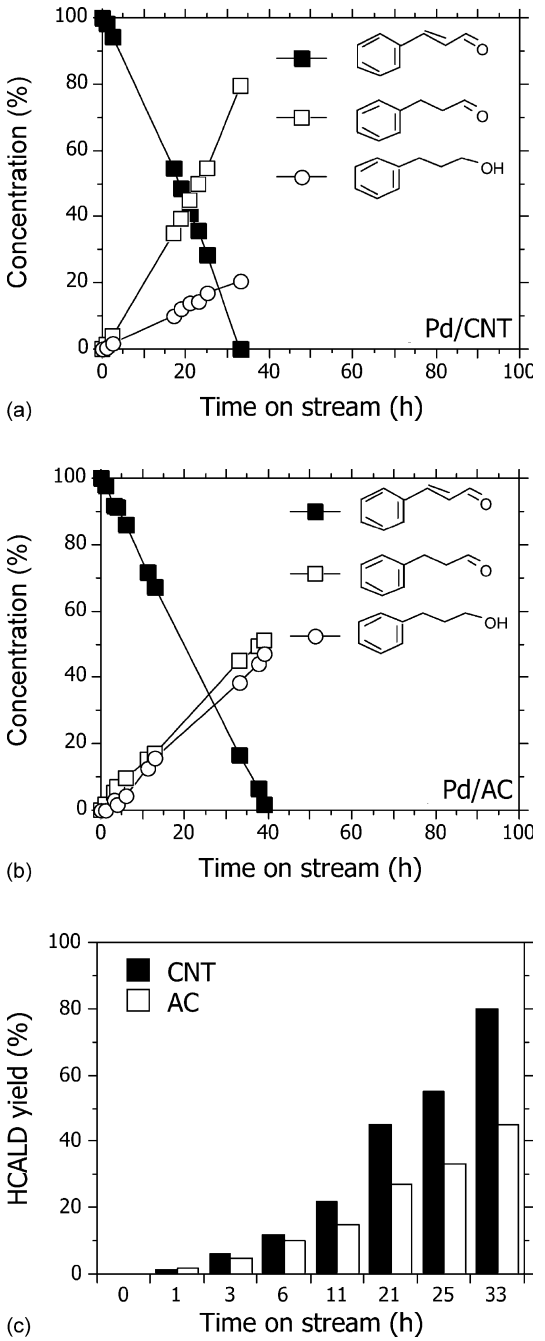

Fig. 14. Cinnamaldehyde concentration and product yields as a function of time on stream obtained at 80 °C over: (a) the CNT supported palladium catalyst and (b) the commercially available catalyst supported on activated charcoal. Comparison of both palladium supported catalysts in terms of yield toward the hydrogenated compounds as a function of time on stream (c).

was. The total absence of any microporosity in the CNT supported catalyst was probably responsible for the significant increase in the selectivity towards the saturated aldehyde. Indeed, microporosity is generally very detrimental to selectivity, leading to an artificial increase in the contact time and allowing successive hydrogenations. The hydrocinnamaldehyde formed first could be adsorbed within the microporosity of the activated charcoal carrier, via the C=O bond, which was strongly weakened after the C=C bond hydrogenation. A rapid removal of the hydrocinnamaldehyde into the liquid phase probably occurred with the CNT supported catalyst, because of the absence of any microporosity. In addition, some residual acidity on the activated charcoal surface could also have favored the further hydrogenation of the weakened C=O bond in the re-adsorbed hydrocinnamaldehyde, according to a consecutive reaction pathway [13,46].

3.3.4. Further objectives for developing nanostructured supports

Recently, it has been reported that carbon nanostructures could be very efficiently used as catalysts for hydrocarbon oxidative dehydrogenation applications when compared to industrial catalysts and other traditional forms of carbon materials [63,64]. However, catalysts usually being composed of a support and one or more active phase compounds, the control and understanding of the active phase deposition process onto a nanostructured support is of great importance for developing this new class of catalysts. It concerns CNTs in terms of particle location (onto the inner and/or outer walls of the material) or morphology. It seemed that the chemical nature of the outer and inner surface of the CNTs could play a very important role, as well as the type of deposition process and chemical pretreatments of the support. For comparison with the CNT supported palladium catalyst, and to illustrate the importance of examining in depth the preparation of catalysts supported on nanotubes, Fig. 15 presents TEM images of the CNT support after the nickel impregnation process and the calcination step. The nickel phase was impregnated as usual by the incipient wetness process of the support with an aqueous solution of nickel nitrate ($Ni(NO_3)_2{\cdot}6H_2O$, Merck). The solid was first dried at 110 °C in air and subsequently calcined at 350 °C for 2 h in order to form the NiO phase. The traditional aqueous impregnation did not allow a very homogeneous dispersion to be obtained, as compared to the palladium deposition reported above (Fig. 12). TEM images showed a very broad particle size distribution, with a lot of CNTs being completely nickel free, whereas nickel particle agglomeration was observed on other tubes and led to big NiO clusters. Isolated bulk NiO particles were also found, without any contact with the carbon support. Work is on going in order to understand phenomena involved in the preparation of such catalysts supported on nanostructured supports (hydrophilic/hydrophobic nature of the surface, role of the precursor salt nature, wetting properties, etc.).

Up to now, very few studies have been devoted to the understanding of the interaction between the deposited active phase and the carbon nanostructure surface. The latter mainly dealt with carbon nanofiber structures, whereas almost no reliable study has investigated the interaction between the active phase and the CNTs surface. The first articles examining the correlation between particle morphology and catalytic performances were by Baker and coworkers [11,13]. The authors reported that nickel decorated carbon nanofibers exhibited a high catalytic activity compared to classical supported catalysts for light hydrocarbon hydrogenation reactions in the gas phase at atmospheric pressure. They suggested that nickel crystallites supported on graphite nanofibers adopted a peculiar hexagonal thin morphology, very different from those observed when nickel was dispersed on classical supports such as silica or alumina. The distribution profile of the nickel particles supported on graphite nanofibers remained very broad, ranging in size from 1.5 to 53.5 nm, with an average of ca. 7–10 nm [11–13]. On the contrary, Planeix et al. [65] have prepared CNT supported ruthenium catalysts, with ruthenium clusters deposited on the external surface of the tubes and exhibiting an homogeneous distribution (particle range in diameter from 3 to 7 nm). The catalyst exhibited a high selectivity towards the C=O bond hydrogenation for the α,β-unsaturated molecule. However, no explanation was put forward by the authors to explain the results. Hoogenraad and coworkers introduced 2.5–3 wt.% of palladium by ion exchange with a Pd–ammonia complex at controlled pH onto carbon nanofibers and nanotubes [66,67]. It was crucial to perform all synthesis steps under nitrogen, especially during the drying, for which extensive

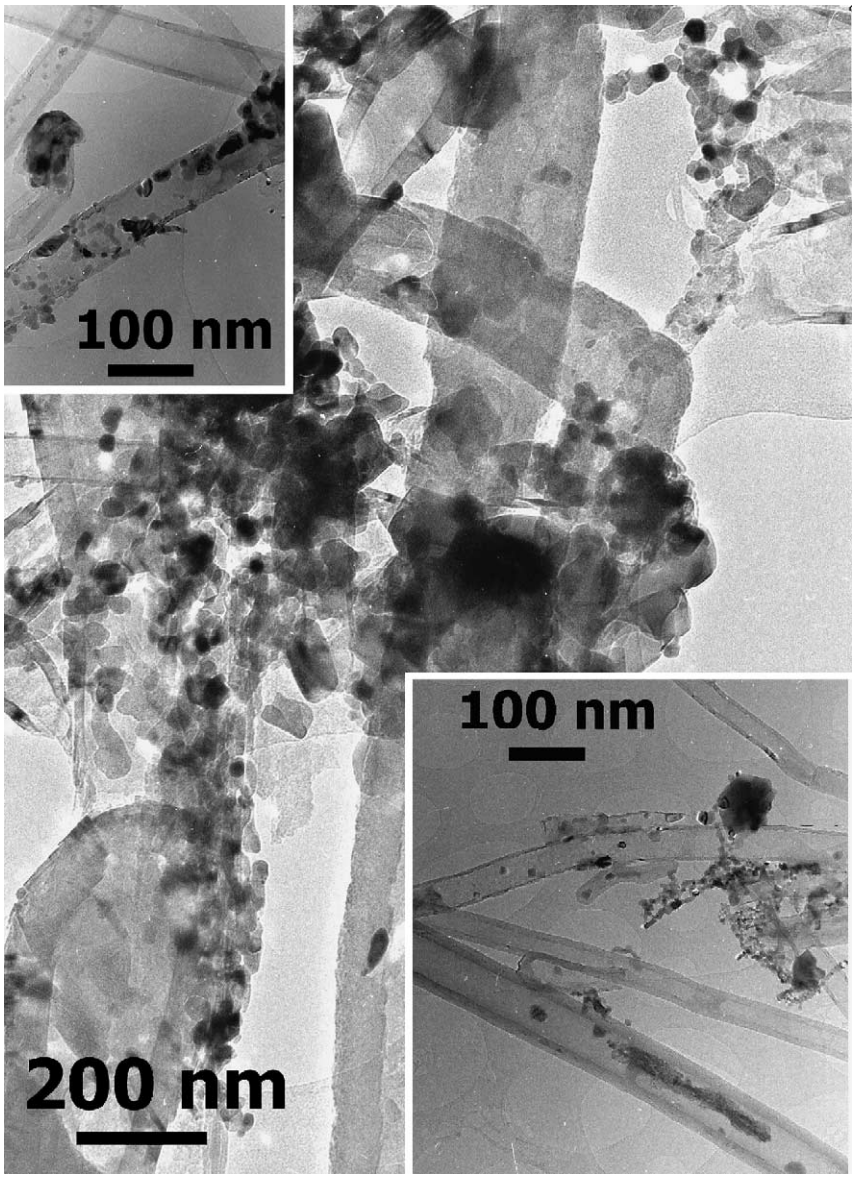

Fig. 15. TEM images of the CNTs after the nickel impregnation process and subsequent calcination in air at 350 °C, evidencing the presence of either encapsulated or supported nickel particles.

sintering of palladium took place. Extended X-ray absorption fine structure and TEM studies evidenced that carefully prepared hydrogen-reduced palladium particles supported on carbon nanofibers had an hemispherical shape, with a mean diameter of 1.5 nm and significant interaction between the support and the palladium. de Jong and Geus [9] have summarized recent work in the research area of active phase deposition.

Several authors have reported interesting work on CNT filling, see for example [68–73]. It is generally thought that such new encapsulated materials will display unusual properties as compared to those of the filled and filling materials and could open new

opportunities in several fields of application, i.e. catalysis, material science, electronic and magnetic storage domains. Ajayan et al. [68] used the surface tension effect to fill CNTs with vanadium oxide at relatively high filling temperature, i.e. 750 °C. However, the filling selectivity remained relatively low, filled and coated CNTs both being observed in the present sample. Che et al. [69] have reported that CNTs, prepared via a combination of chemical vapor deposition and template-synthesis using an alumina membrane, could be efficiently filled with nanoclusters of Pt or Pt/Ru with a mean diameter of around 5 nm for Pt and 1.5 nm for the Pt/Ru alloy. Template techniques were also used to prepare platinum or iron filled CNTs in which the metal or metal oxide was present as nanorods or nanoparticles [70–72]. Recently, Xu et al. [73] evidenced the filling of single-walled CNT with a lanthanide halide element, by heating an intimate mix of CNT and the halide above the melting point of this latter. The control of the metal deposition (for example as nanowires) in the tubes was, up to now, a crucial challenge for potential applications in magnetic recording technology. In the catalysis field, and looking for nanoparticles instead of nanowires, the possibility to rationally control by means of mild preparation methods the active phase deposition in terms of location in or on the nanostructured support, particle size and morphology, will now become more and more important for the development of this new class of catalysts. Finally, the application of the SMS method presented above for the synthesis of various kinds of carbide nanotubes or nanowires which could display peculiar (catalytic) properties compared to traditional materials, will be also an exciting and profitable challenge in either catalysis or materials applications for the future. Combination of the confinement effect put forward above, the tubular morphology and the high mechanical strength of the CNTs will be also extended to the synthesis of materials under peculiar conditions as compared to those usually encountered up to now.

4. Conclusion

The above results clearly show the high performances of nanostructured carbon and carbide materials, as compared to those usually obtained with the traditional macroscopic supports. Combination of a tubular morphology and the high external surface of these supports rendered them superior in terms of catalytic performance and also significantly influenced the selectivity pattern of the reaction.

The low temperature selective oxidation of H_2S contained in Claus Plant Tail-Gas Units in relatively large amounts (almost 0.2 vol.%) is probably not the most appropriate process for a potential industrial application using such new supported catalysts. However, it has enabled the new concept of inner partial pressure, i.e. confinement effect, to be developed. In the case of H_2S removal, but more generally for other polar molecules, it could be very efficiently used to remove the last residual traces (in the ppm range), for which processes are seriously limited kinetically by the very low partial pressure of the molecules to be treated. Such a confinement effect will also be proposed to explain very interesting results in the field of material and catalyst synthesis which will soon be published. In the hydrogenation field, the carbon nanostructured material also exhibited an interesting behavior towards selective C=C bond hydrogenation as compared to that obtained on the commercial activated charcoal catalyst, despite the large difference in terms of the support surface area. The high selectivity obtained over the CNT-based catalyst was attributed to the complete absence of micropores and residual acidic sites in the support matrix. Such peculiar properties seem to be most promising for the future class of catalysts which will have to cope with the more and more demanding selective reactions, in order to reduce waste coming from further purification processes.

Although carbon and more recently SiC nanostructures have been efficiently used, such materials have now to deal with detrimental synthesis limitations. de Jong and Geus agreed in their recent review that facilities to provide carbon nanostructures in larger amounts could now allow the creation of the required driving force in order to significantly decrease the production costs and also to overcome the present synthesis limitations [9]. It is worth noting that the large scale synthesis of carbon nanofibers with a controlled diameter of about 50 nm was very recently achieved at relatively low temperature (550–650 °C) using a simple catalytic process [36]. The synthesized carbon nanofibers could also be used as a catalyst support without subsequent purifications, due to the

use of CNTs as support, the high nanofiber yields and the high purity obtained. Recently, the laboratory has reported a new preparation method which allowed carbon nanostructured material composites to be obtained, which displayed similar properties to those of pristine materials and easy handling and packing similar to those encountered for macroscopic materials [74,75]. The last catalytic application for the gaseous decomposition reaction, i.e. $N_2H_4 \rightarrow N_2 + 2H_2$, over such a new composite seemed to be extremely promising. For the carbide field, the newly formed SICAT company is now deeply involved in the development of medium surface area SiC-based materials [76].

Acknowledgements

The authors would like to acknowledge Dr. C. Estournès (IPCMS, GMI, Strasbourg) and Dr. Ph. Vennégues (CRHEA, Sophia-Antipolis) for performing some of the SEM analyses. Lurgi GmbH and ADEME (J.-M.N.), INPE (R.V.), Conoco (J.-P.T.) and the Educational Ministry (L.P.) are gratefully acknowledged for providing grants to support part of the present work.

References

[1] M.F.M. Zwinkels, S.G. Jaras, P.G. Menon, T.A. Griffin, Catal. Rev.-Sci. Eng. 35 (1993) 319.
[2] P. Burtin, J.P. Brunelle, M. Pijolat, M. Soustelle, Appl. Catal. 34 (1987) 239.
[3] J.A. Schwartz, C. Contescu, A. Contescu, Chem. Rev. 95 (3) (1995) 475.
[4] H.C. Yao, H.K. Stepien, H.S. Gandhi, J. Catal. 61 (1980) 547.
[5] S. Iijima, Nature (London) 354 (1991) 56.
[6] T.W. Ebbesen (Ed.), Carbon Nanotubes: Preparation and Properties, CRC Press, Boca Raton, 1997.
[7] M. Terrones, W. Kuang Hsu, H.W. Kroto, D.R.M. Walton, Top. Curr. Chem. 199 (1999) 189. and references therein.
[8] P.M. Ajayan, Chem. Rev. 99 (1999) 1787.
[9] K.P. de Jong, J.W. Geus, Catal. Rev.-Sci. Eng. 42 (4) (2000) 481.
[10] P.M. Ajayan, O.Z. Zhou, in: M.S. Dresselhaus, G. Dresselhaus, Ph. Avouris (Eds.), Carbon Nanotubes: Synthesis, Structures, Properties and Applications, Topics in Applied Physics, vol. 80, Springer, Heidelberg, 2001, pp. 391–425.
[11] A. Chambers, T. Nemes, N.M. Rodriguez, R.T.K. Baker, J. Phys. Chem. B 102 (1998) 2251.
[12] C. Park, R.T.K. Baker, J. Phys. Chem. B 102 (1998) 5168.
[13] F. Salman, C. Park, R.T.K. Baker, Catal. Today 53 (1999) 385.
[14] C. Pham-Huu, N. Keller, L.J. Charbonnière, R. Ziessel, M.J. Ledoux, Chem. Commun. 19 (11) (2000) 1871.
[15] C. Pham-Huu, N. Keller, G. Ehret, L.J. Charbonnière, R. Ziessel, M.J. Ledoux, J. Mol. Catal. A: Chem. 170 (2001) 155.
[16] M.J. Ledoux, C. Pham-Huu, R.R. Chianelli, Curr. Opin. Solid State Mater. Sci. 1 (1996) 96.
[17] M.A. Vannice, Y.L. Chao, R.M. Friedman, Appl. Catal. 20 (1986) 91.
[18] P.W. Lednor, Catal. Today 15 (1992) 241.
[19] R. Moene, H.T. Boon, J. Schooman, M. Makkee, J.A. Moulijn, Carbon 34 (1996) 567.
[20] M. Boutonet-Kizling, P. Stenius, S. Andersson, A. Frestad, Appl. Catal. B: Environ. 1 (1992) 149.
[21] M.J. Ledoux, S. Hantzer, J. Guille, D. Dubots, US Patent 4 914 070 1990.
[22] M.J. Ledoux, S. Hantzer, C. Pham-Huu, J. Guille, M.P. Desaneaux, J. Catal. 114 (1988) 176.
[23] M.J. Ledoux, C. Pham-Huu, Catal. Today 15 (1992) 263.
[24] N. Keller, C. Pham-Huu, S. Roy, M.J. Ledoux, C. Estournès, J. Guille, J. Mater. Sci. 34 (1999) 3189.
[25] C. Pham-Huu, S. Marin, M.J. Ledoux, M. Weibel, G. Ehret, M. Benaïssa, E. Peschiera, J. Guille, Appl. Catal. B: Environ. 4 (1994) 45.
[26] P. Del Gallo, Ph.D. Dissertation, Louis Pasteur University of Strasbourg, France, 1995.
[27] C. Pham-Huu, P. Del Gallo, E. Peschiera, M.J. Ledoux, Appl. Catal. A: Gen. 132 (1995) 77.
[28] B. Heinrich, Ph.D. Dissertation, Louis Pasteur University of Strasbourg, France, 1999.
[29] E.M. Harlin, A.O.I. Krause, B. Heinrich, C. Pham-Huu, M.J. Ledoux, Appl. Catal. A: Gen. 185 (1999) 311.
[30] N. Keller, Ph.D. Dissertation, Louis Pasteur University of Strasbourg, France, 1999.
[31] N. Keller, C. Pham-Huu, C. Crouzet, M.J. Ledoux, S. Savin-Poncet, J.-B. Nougayrède, J. Bousquet, Catal. Today 53 (1999) 535.
[32] M.J. Ledoux, C. Pham-Huu, N. Keller, S. Savin-Poncet, J.-B. Nougayrède, J. Bousquet, W. Boll, R. Morgenroth, Sulphur 269 (2000) 41.
[33] N. Keller, C. Pham-Huu, M.J. Ledoux, Appl. Catal. A: Gen. 217 (2001) 205.
[34] N. Keller, C. Pham-Huu, C. Estournès, M.J. Ledoux, Catal. Lett. 61 (1999) 151.
[35] M.J. Ledoux, C. Pham-Huu, N. Keller, J.-B. Nougayrède, S. Savin-Poncet, J. Bousquet, Catal. Today 61 (2000) 157.
[36] C. Pham-Huu, N. Keller, V.V. Roddatis, G. Mestl, R. Schlögl, M.J. Ledoux, Phys. Chem.-Chem. Phys. 4 (3) (2002) 514.
[37] H. Jaeger, T. Behrsing, Compos. Sci. Technol. 51 (1994) 231.
[38] N.M. Rodriguez, J. Mater. Res. 8 (1993) 3233.
[39] J.W. Geus, A.J. van Dillen, M.S. Hoogenraad, Mater. Res. Soc. Symp. Proc. 368 (1995) 87.
[40] N. Keller, C. Pham-Huu, M.J. Ledoux, C. Estournès, G. Ehret, Appl. Catal. A: Gen. 187 (1999) 255.
[41] M.J. Ledoux, C. Pham-Huu, Cattech 4 (2002) 226.

[42] E. Peschiera, Ph.D. Dissertation, Louis Pasteur University of Strasbourg, France, 1993.
[43] M.J. Ledoux, N. Keller, H. Lamprell, C. Pham-Huu, B. Heinrich, C. Estournès, M.E. Harlin, in: Proceedings of the Seventh International Symposium on Scientific Bases for the preparation of Heterogeneous Catalysts, Stud. Surf. Sci. Catal. 118 (1995) 855.
[44] J.H. de Boer, in: D.H. Everett (Ed.), The Structure and Properties of Porous Materials, 1958.
[45] R.S.H. Mikhail, S. Brunauer, E.E. Bodor, J. Coll. Int. Sci. 26 (1968) 45.
[46] L. Zhang, J.M. Winterbottom, A.P. Boyes, S. Raymahasang, J. Chem. Technol. Biotechnol. 72 (1998) 264.
[47] S. Galvagno, A. Donato, G. Neri, R. Pietropaolo, D. Pietropaolo, J. Mol. Catal. A: Chem. 48 (1989) 223.
[48] S. Galvagno, G. Capannelli, G. Neri, A. Donato, R. Pietropaolo, D. Pietropaolo, J. Mol. Catal. A: Chem. 64 (1991) 237.
[49] S. Galvagno, A. Donato, G. Neri, R. Pietropaolo, D. Pietropaolo, J. Mol. Catal. A: Chem. 78 (1993) 227.
[50] B. Coq, P.S. Kumbhar, C. Moreau, P. Moreau, M.G. Warawdekar, J. Mol. Catal. A: Chem. 85 (1993) 215.
[51] V.P. Dravid, X. Lin, Y. Wang, A. Yee, J.B. Keterson, R.P.H. Chang, Science 259 (1993) 1601.
[52] N. Hatta, K. Murata, Chem. Phys. Lett. 217 (1994) 398.
[53] Y. Ando, J. Appl. Phys. 32 (1993) L1342.
[54] P.M. Ajayan, Chem. Mater. 11 (1999) 3862.
[55] C. Bouchy, Ph.D. Dissertation, Louis Pasteur University of Strasbourg, France, 1998.
[56] A. Pieplu, O. Saur, J.C. Lavalley, Catal. Rev.-Sci. Eng. 40 (1998) 409.
[57] A.C. Dillon, K.M. Jones, T.A. Bekkedahl, C.H. Klang, D.S. Bethune, M.J. Heben, Nature 386 (1997) 377.
[58] C. Liu, Y.Y Fan, M. Liu, H.T. Cong, H.M. Cheng, M.S. Dresselhaus, Science 286 (1999) 1127.
[59] J.M. Bonard, L. Forro, D. Ugarte, W.A. de Herr, A. Châtelain, Eur. Chem. Chronicle 1 (1998) 9.
[60] D. Ugarte, A. Châtelain, W.A. de Herr, Science 274 (1996) 1897.
[61] N.M. Rodriguez, A. Chambers, R.T.K. Baker, Langmuir 11 (1995) 3862.
[62] M.-S. Kim, N.M. Rodriguez, R.T.K. Baker, Mater. Res. Soc. Symp. Proc. 368 (1995) 99.
[63] G. Mestl, N.I. Maksimova, N. Keller, V.V. Roddatis, R. Schlögl, Angew. Chem. 113 (11) (2001) 2122;
G. Mestl, N.I. Maksimova, N. Keller, V.V. Roddatis, R. Schlögl, Angew. Chem. Int. Ed. 40 (11) (2001) 2066.
[64] N. Keller, N.I.N.I. Maksimova, N.V.V. Roddatis, V.V.M. Schur, R.G. Mestl, Y.V. Butenko, V.L. Kuznetsov, R. Schlögl, Angew. Chem. 114 (11) (2002) 1962;
N. Keller, N.I. Maksimova, V.V. Roddatis, M. Schur, G. Mestl, Y.V. Butenko, V.L. Kuznetsov, R. Schlögl, Angew. Chem. Int. Ed. 41 (11) (2002) 1885.
[65] J.M. Planeix, N. Coustel, B. Coq, V. Brotons, P.S. Kumbhar, R. Dutartre, P. Geneste, P. Bernier, P.M. Ajayan, J. Am. Chem. Soc. 116 (1994) 7935.
[66] M.S. Hoogenraad, Ph.D. Dissertation, Utrecht University, The Netherlands, 1995.
[67] B.J. Mojet, M.S. Hoogenraad, A.J. van Dillen, J.W. Geus, D.C. Köningsberger, J. Chem. Soc., Faraday Trans. 93 (1997) 4371.
[68] P.M. Ajayan, O. Stephan, Ph. Redlich, C. Colliex, Nature 375 (1995) 564.
[69] G. Che, B.B. Lakshmi, C.R. Martin, E.R. Fisher, Langmuir 15 (1999) 750.
[70] T. Kyotani, L. Tsai, A. Tomita, Chem. Commun. 7 (1997) 701.
[71] B. Lakshmi, E.R. Fisher, C.R. Martin, Nature 393 (1998) 346.
[72] B.K. Pradhan, T. Toba, T. Kyotan, A. Tomita, Chem. Mater. 10 (1998) 2510.
[73] C. Xu, J. Sloan, G. Brown, S. Bailey, V.C. Williams, S. Friedrichs, K.S. Coleman, E. Flahaut, J.L. Hutchison, R.E. Dunin-Borkowski, M.L.H. Green, Chem. Commun. 24 (2000) 2427.
[74] C. Pham-Huu, R. Vieira, M.J. Ledoux, L. Charbonnière, R. Ziessel, Demande de Brevet Français No. 01-15178, assigned to SICAT.
[75] R. Vieira, C. Pham-Huu, N. Keller, M.J. Ledoux, Chem. Commun. (2002) 954.
[76] Claude Job, SICAT, Paris, France.